Available online at www.sciencedirect.com

ScienceDirect

Procedia CIRP 137 (2025) 277–282

www.elsevier.com/locate/procedia

CIRP Conference on Electro Physical and Chemical Engineering

General applicability of fatigue life assessment method for metal laser powder bed fusion parts: Variation in material, shape and test conditions

Wessel W. Wits[a,b,*] and Emiel Amsterdam[a]

[a]*Metal Additive Manufacturing Technology Centre (MAMTeC), NLR - Royal Netherlands Aerospace Centre, Marknesse, the Netherlands*
[b]*Faculty of Electrical Engineering, Mathematics and Computer Science, University of Twente, Enschede, the Netherlands*

* Corresponding author. *E-mail address:* w.w.wits@utwente.nl

Abstract

The general applicability of our formerly developed fatigue prediction and life assessment methodology for metal Laser Powder Bed Fusion (LPBF) parts is validated for a new commonly used feedstock material; AlSi7Mg. Moreover, another specimen geometry and surface finish, as well as another fatigue loading condition have been used. The fatigue life assessment method for additively fabricated metal parts uses both the size of LPBF-process inherent initial defects and a material- and process-specific pivot point to accurately predict the fatigue life. An experimental campaign was completed and confirmed that the method is indeed expandable to another material, shape and fatigue loading condition.

Keywords: Additive Manufacturing; Laser powder bed fusion; Fatigue; Effect of defect; Fatigue life assessment; *S-N* curves

1. Introduction

Additive Manufacturing (AM), commonly referred to as 3D printing, has experienced significant growth in recent decades and has established itself as an accepted fabrication technique within various industries [1]. Evolving from its origins in rapid prototyping and tool making, AM has progressed to encompass the fabrication of complete parts, assemblies and products. Amongst various AM processes, Laser Powder Bed Fusion (LPBF) stands out as the predominant fabrication process for complex metallic components [2]. However, the widespread adoption of metal LPBF in industry is primarily confined to static and non-critically loaded components. In the case of critically loaded components, where a thorough assessment of the fatigue strength is essential, the reliability of metal LPBF remains a challenge [3]. Under a single optimized process parameter set, LPBF parts are known to exhibit a stochastic distribution of mechanical properties largely due to local differences in thermal history [4]. LPBF-process inherent defects are localized stress concentrators and result in significant variability in fatigue life data, complicating the evaluation of structural integrity over the operational life of fabricated components [5]. Despite extensive reporting on defect detection, the influence of these defects on fatigue performance has yet to be fully understood.

The most common intrinsic defects found in LPBF parts are typically categorized into two types: i) irregular Lack of Fusion (LoF) defects and ii) more spherical porosity defects [6, 7]. LoF defects are irregular crack-like anomalies that elongate between layers resulting from suboptimal process parameters or insufficient energy input between adjacent layers. In contrast, porosity defects exhibit a relatively regular and smooth spherical surface, arising from factors like inert gas entrainment, vapour recoil, keyhole collapse and others. Both types of defects may act as crack nucleation sites; however, due to their crack-like appearance, LoF defects are much more detrimental for fatigue performance [8].

To predict the fatigue life of LPBF parts, this author team has previously presented a method that takes the size of such inherent initial defects into account [9]. The method is based on

10.1016/j.procir.2025.02.267

the industry-accepted empirical stress-life approach that makes use of *S-N* curves also known as Wöhler curves [10]. At the core of this approach it is assumed that at a low number of cycles the alternating stress is independent of the initial material state, such as surface roughness or surface defects. Conversely, at a high number of cycles an infinite life threshold is predicted by the fatigue or endurance limit, S_e, and knockdown factors lowering the endurance limit based on the initial material state are readily provided in literature [11]. In this paper, we follow a similar strategy in which the size of inherent initial defects of an LPBF part is taken into account to predict its fatigue performance. We assume that an increasing size of initial defects leads to a lower fatigue life. Moreover, similarly to the stress-life approach, we also assume that there is a point at which the fatigue life is independent of the material's initial condition. This point, which is projected in Figure 1 as the pivot point, is material and process specific, and must be determined experimentally. Note that, in contrast to Wöhler curves, custom to scientific consistency the independent (predictor) variable, here the maximum stress, S_{max}, is indicated on the *x*-axis and the dependent (response) variable, in this case the fatigue life in cycles to failure, *N*, is indicated on the *y*-axis. The black dots and lines refer to the results of our previous study [9] using the following conditions: AlSi10Mg as material of choice, a circular Ø3 mm machined and polished test specimen, and a force-controlled, tension-tension constant amplitude axial loading condition with a fatigue stress ratio ($R = S_{min}/S_{max}$) of 0.1.

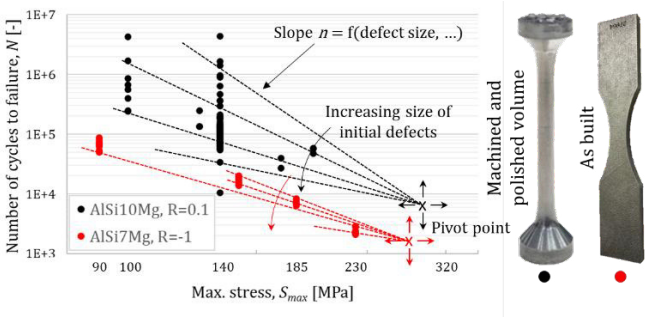

Fig. 1. Exemplary fatigue (*S-N*) curves for different materials, different specimen types and different testing conditions in which the slope through a material's pivot point is a function of the initial defect size.

Our previous study proved that for AlSi10Mg there indeed exists a pivot point at 2,000 cycles and 310 MPa that can accurately predict the fatigue life based on the initial defect size and stress within an LPBF part [9]. In this paper, we seek to validate the applicability of our developed method for another material, test specimen geometry, surface quality and stress ratio. More damaging fatigue life conditions, leading to a significant lower life, are introduced to examine how far the applicability of the method can be stretched. This is illustrated by the red dots and lines in Figure 1 showing fatigue lives as low as 2,000 cycles. High maximum stresses and a fully reversed stress ratio of R = -1, compared to the positive stress ratio (R = 0.1) of the former study, are used. Moreover, the LPBF specimens are tested in a relatively rough 'as built' condition rather than being mirror polished. Based on initial defect sizes from fracture surface analyses, the pivot point is determined by utilizing the model to predict the fatigue lives and compare them to the measured fatigues lives for the new material and new set of test conditions.

Nomenclature

a	empirical constant
b	empirical constant
d	initial defect size [µm]
N	number of cycles to failure [-]
N_{meas}	measured number of cycles to failure [-]
N_{pivot}	number of cycles to failure at the pivot point [-]
N_{pred}	predicted number of cycles to failure [-]
n	slope of *S-N* curve through the pivot point [MPa^{-1}]
R	fatigue stress ratio [-]
R_a	surface roughness [µm]
S	stress [MPa]
S_e	fatigue or endurance limit [MPa}
S_{max}	maximum stress [MPa]
S_{min}	minimum stress [MPa]
S_{pivot}	stress at the pivot point [MPa]

2. Methodology

To validate the developed fatigue life assessment method, an experimental test campaign was devised. AlSi7Mg was selected as feedstock material. Compared to AlSi10Mg of the previous study, the lower silicon volume fraction of AlSi7Mg causes a weaker solid-solution hardening effect resulting in a lower tensile strength, but increased ductility [12]. In total 54 test specimens according to the geometry of Figure 2(a) were fabricated in three separate build jobs using the material-specific optimized LPBF parameter set. The continuous radius at the gauge section, compared to the previously cylindrical shape, will result in a (net-section) stress concentration factor of 1.06 and, hence, a stress gradient at the edges of the specimen [13].

The test specimens were fabricated at an inclination angle of 55°, as indicated in Figure 2(b), on a FormUp 350 system and received a stress relieve heat treatment afterwards. No additional post-processing was applied; hence, the samples are considered in the 'as built' surface condition, as depicted in Figure 2(c). Again compared to the previous study, both the inclination angle introducing overhang defects compared to a vertical build and a rough 'as built' specimen compared to a polished sample will result in a lower fatigue life.

The first build job consisted of six test specimens, of which the up- and downskin parameters of the inclined build direction were intentionally adjusted to create more defects and a higher surface roughness in the (sub)surface region, as proximity to the surface is known to be a critical parameter for fatigue resistance [14]. This first set of samples is used to determine the pivot point; hence, both fatigue testing and fracture surface analysis are performed. The second and third build job consisted of 24 specimens each. The latter two build jobs were fabricated without adjusting the up- and downskin parameters. The fatigue test results of these specimens are used to validate the method.

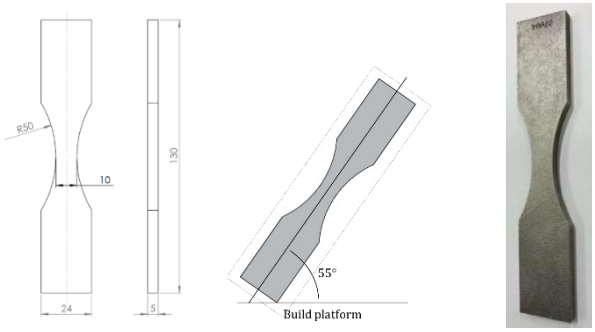

a) specimen geometry b) build direction c) fabricated part

Fig. 2. Definition and fabrication approach of fatigue test specimen.

After specimen production, the surface roughness was determined for the four vertical sides of each specimen. Fatigue testing was performed on an MTS fatigue testing machine. All specimens were subjected to a tension-compression axial loading condition with a fully-reversed stress ratio (R = -1). The six specimens of the first build job with adjusted up- and downskin parameters were tested at a (net-section) maximum stress, S_{max}, of 90 and 150 MPa to obtain cycles to failure in the High Cycle Fatigue (HCF) regime. The test frequency was set to 10 Hz and the number of cycles to failure was recorded.

After failure, fracture analysis was performed by optical investigation of each fracture surface. The location of the fatigue crack in the test specimen, as well as the size of the initial defect at the crack nucleation site were determined by optical microscopy. The major axis of the initial defect was determined as the initial defect size. Localized stress concentrations may be caused by a range of parameters; however, in this study the major axis of the observed initial defect is assumed as first-order size parameter governing the fatigue life [9, 15, 16].

The second and third 2x 24 validation specimens were tested at maximum stresses of 90, 150, 185 and 230 MPa representing a cyclic stress of approximately 25 to 60% of the Ultimate Tensile Strength (UTS). In seven instances the test specimen did not fail and a run out was observed. This only occurred at the higher stress levels of 185 and 230 MPa, where the maximum number of cycles to be tested was set to 9,000 and 3,000 cycles, respectively. These seven measurements were taken out of the dataset leaving 41 measurements in the validation set.

The fatigue life is modelled according to the *S-N* curves of Figure 1. As the curves are double logarithmic, a power law function is used to express the predicted number of cycles to failure:

$$N_{pred} = N_{pivot} \cdot \left(\frac{S_{max}}{S_{pivot}}\right)^{n} \quad \text{with} \quad n = a \cdot d^{b} \qquad (1)$$

where, the subscript pivot refers to the pivot point that needs to be determined experimentally. The slope, n, always going through the pivot point, is a power law function of the initial defect size, d, and two constants a and b that are statistically determined by regression analysis. To quantify the parameters of Equation (1) a number of steps must be undertaken as part of an iterative process, as explained in our previous publication [9]. For the sake of brevity, the essential steps are discussed in short here.

First, an initial set of specimens is used to determine the pivot point at which location the initial defect size is insignificant with respect to the fatigue life. This pivot point is thereafter used to determine the slope, n, of the initial set. In this study, the maximum stress at the pivot point, S_{pivot}, is assumed to be equal to the UTS, which leaves the number of cycles to failure at the pivot point, N_{pivot}, as the only fit parameter of the model. For each measurement the slope, n, can be computed for a given N_{pivot}. By regression analysis of the power law relation between the computed slopes and associated initial defect sizes, constants a and b of Equation (1) are determined.

Second, Equation (1) is used to predict the fatigue life of each test specimen and compared to the measured fatigue life. As predicted and measured lives should be equal, a proportional relationship is expected where both the proportionality constant and the exponent are equal to unity ($y = 1 \cdot x^{1}$). By iteratively adjusting the pivot point, the error of the proportional relationship is minimized resulting in the final empirical formulation of Equation (1) for a given material, test specimen geometry, surface condition and fatigue test condition.

In this paper, a novel addition to the methodology is presented, in which the fatigue results of a second (and third) set of specimens is used to construct an average *S-N* curve. This curve is used to validate the afore empirically quantified Equation (1).

3. Results and discussion

Table 1 lists the measured surface roughness values of the four vertical sides of each specimen, while Table 2 reports the average surface roughness of the validation set. As intended, the adjusted up- and downskin parameters result in higher average surface roughness values for each of the four vertical sides. In particular the up- and downskin surfaces show a significant rise in average surface roughness of 175% and 42%, respectively. Although, the front side and to a lesser extend the back side are also affected by the change in processing parameters.

Table 1. Measured roughness (R_a) of four vertical sides of the six initial specimens [µm]; note that front is the labeled side as oriented in Figure 2(c).

Specimen	Upskin side	Downskin side	Front	Back
I	11.9	11.3	8.3	8.2
II	14.5	11.4	14.4	8.8
III	12.9	9.8	7.9	10.2
IV	19.2	19.3	14.3	10.7
V	11.6	11.5	11.6	10.5
VI	13.0	14.2	11.4	7.7
Average	13.9	12.9	11.3	9.4

Table 2. Measured average roughness (R_a) of four vertical sides of the validation set [µm].

	Upskin side	Downskin side	Front	Back
Average	5.0	9.1	6.9	8.0

The pivot point is assumed to be at the material's UTS, in this case at 382 MPa. Therefore, only the number of cycles to failure at the pivot point needs to be determined iteratively. This is illustrated in Figure 3 by the two vertical arrows. The six failed test specimens of the first build job with adjusted up- and downskin parameters and rough 'as built' surfaces are depicted as well in the figure inset. As the fracture is not always at the minimum gauge section of the test specimen, the nominal stress at the crack location is used instead of the nominal stress at the lowest cross section. For instance, for Specimens I & VI which failed relatively far away from the centre and hence have a larger cross section, the maximum stress in Figure 3 is plotted lower than the nominally configured stresses of 150 and 90 MPa, respectively.

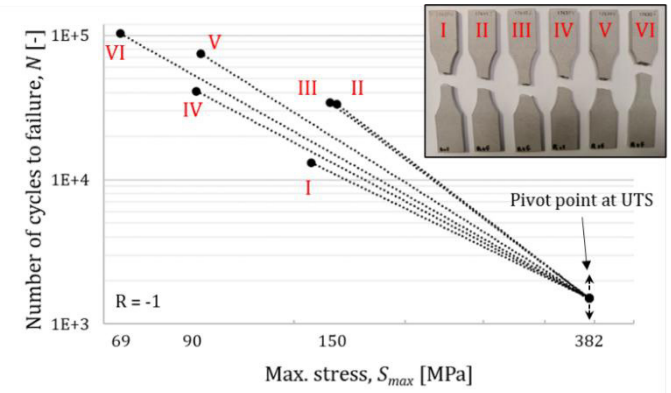

Fig. 3. Fatigue results of the six test specimens (see inset) of the first build job with adjusted up- and downskin parameters.

According to the method, for each specimen of Figure 3 the corresponding slope through an iteratively optimized pivot point can be determined following:

$$n = \frac{log_{10}(N_{meas}) - log_{10}(N_{pivot})}{log_{10}(S_{max}) - log_{10}(S_{pivot})} \quad (2)$$

In Figure 4 the computed slopes are associated to the measured initial defect sizes. Although processing conditions were similar for all six specimens, the initial defect sizes range from 380 µm to 680 µm and attest to the aforementioned stochastic nature of the LPBF process. The defect sizes are relatively high compared to the reported state of the art [17]. Also, the defect sizes are large compared to the measured average surfaces roughness values (see Table 1). In all cases however the initial defect was near the surface as can be expected from the adjusted up- and downskin process parameters and as is commonly the case with fatigue failures.

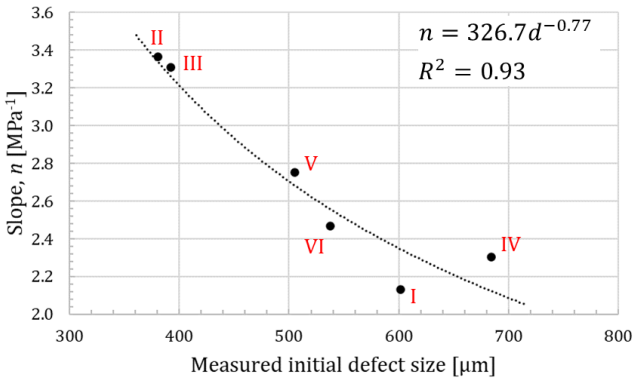

Fig. 4. Statistically determined slope as a function of the initial defect size assuming a pivot point at UTS and 1509 cycles to failure.

The power law relation between the slope and initial defect size is indicated in Figure 4 by the black line. With the exception of Specimen IV, the results show that a larger initial defect size leads to a lower slope, as one may expect. By linear regression, constants a and b, are determined to be 326.7 and -0.77, respectively, for the optimal pivot point of (UTS, 1509 cycles) as obtained in the subsequent paragraph. The coefficient of determination R^2, providing a measure for the fit quality, is 93%.

With Equation (1) quantified as shown in the Figure 5 inset, the model is used to predict the number of cycles to failure based on the initial defect size, d, and maximum stress, S_{max}. Figure 5 shows the result of each of the six test specimens. The optimal pivot point was iteratively determined to be at 1509 cycles to failure and UTS. At this location, the proportionality constant and exponent are both unity with a fit quality of 95%, as also shown in the figure.

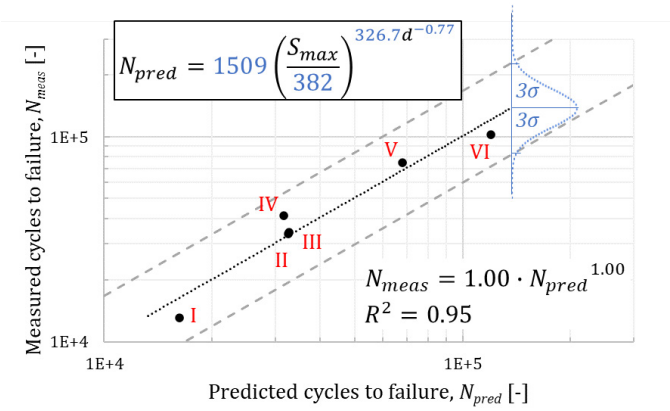

Fig. 5. Correlation between the measured and predicted number of cycles to failure with a proportionality constant and exponent of unity.

The dashes grey lines in Figure 5 indicated the 6σ statistical confidence band accounting for 99.73% of observations around the mean. As visualized all tested specimens fall well within the bounds. In fact, the largest offset was Specimen IV at 1.5σ from the mean. The model is capable to accurately predict fatigue performance even though the range of initial defect sizes is relatively large ranging from 380 µm to 680 µm (see Figure 4), the stochastic nature of the LPBF process [4] and the high 'as built' surface roughness condition of the tested specimens (see

Table 1). This demonstrates the prominent value of the method. For a known material and process parameter set, the fatigue performance of a part can be predicted by a priori detecting its maximum defect size e.g. by non-destructive X-ray Computed Tomography (XCT).

Figure 6 depicts the fracture surfaces of Specimens II & IV having the smallest and largest initial defect sizes, respectively. The figure highlights the initial defect location and initial defect size as reported in Figure 4. As indicated in the figure, the initial defect sizes of Specimens II & IV are 380.9 µm and 683.8 µm, respectively. Both defects originate at the external perimeter, although Specimen II failed from the front surface in contrast to Specimen IV, which failed from the side.

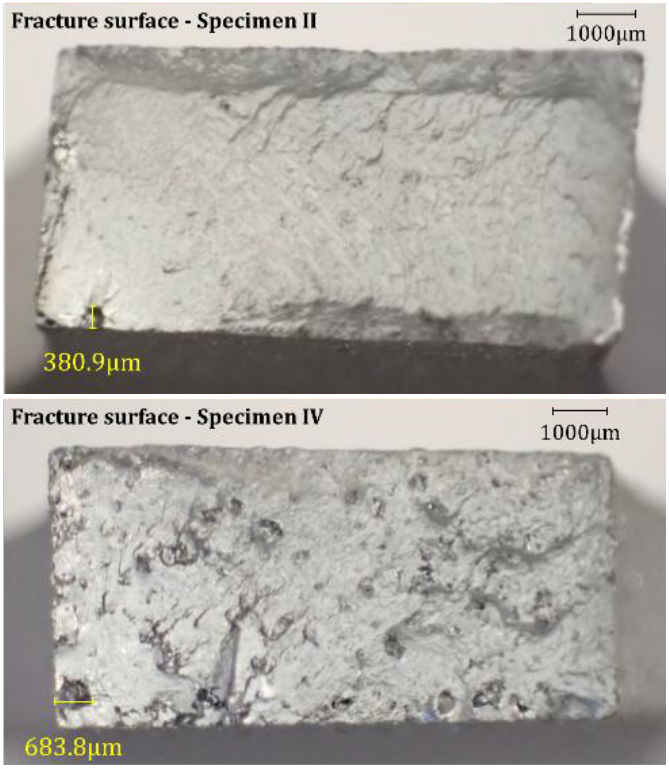

Fig. 6. Fracture analysis of Specimen II (top) and Specimen IV (bottom).

The predicted and measured lives of Specimens II & IV are relatively similar (see Figure 5) although they were tested at 150 and 90 MPa, respectively. In fact, the initial defect sizes of these specimens are the smallest and largest, respectively (see Figure 4). Hence, the difference the defect size is responsible for the similar fatigue life assessment. From the fracture surfaces of Figure 6, it can also be observed that the fabrication quality of Specimen IV is lower compared to Specimen II explaining the larger initial defect size. As process parameters were similar, the difference in surface condition may be attributed to other parameters such as the location on the build plate, local thermal effects during the build job or other unknown LPBF effects.

Finally, to validate the quantified model, the fatigue results of the validation set are presented in Figure 7 based on the net-section stress of the minimum cross-section. The blue markers indicate the initial six specimens of which the fracture surface was analysed in order to determine the material- and process-specific pivot point. Left and right of the pivot point, the 3σ bounds of the determined UTS are given by the blue dashed lines and provide a statistical measure for the predicted value. Also, two power law regressions are shown. The red line indicates the regression for all tested specimens, while the black line only indicates the regression for the specimens in the HCF regime, i.e. with > 10^4 cycles to failure.

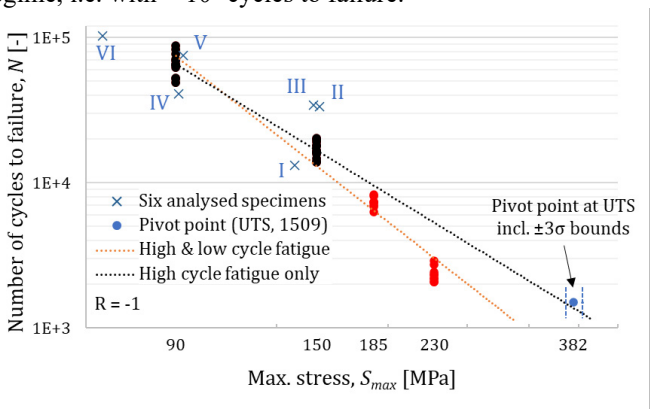

Fig. 7. Measured fatigue life of 41 specimens of the validation set.

For the HCF results (see black line), the fitted *S-N* curve goes through the afore determined pivot point. The combined high and low cycle fatigue results are not fitted well with a power law relationship. This is illustrated by the red line which is not representative of the measured results due to the inclusion of low cycle fatigue failures with < 10^4 cycles to failure. Here, at 150 and 230 MPa the cycles to failure are under- and overpredicted, respectively. The current fatigue prediction methodology is developed using specimens in which the fatigue crack is growing in a uniform stress field from the initial defect size all the way up to complete failure. It is possible that in this case for AlSi7Mg, with an experimentally determined 0.2% offset yield stress of 260 MPa, the stress from the stress concentration at 185 and 230 MPa net-section maximum stress results in local plasticity. This would change the stress gradient in the specimens that are tested at these maximum stresses compared to the ones tested at 90 and 150 MPa, resulting in lower fatigue lives than expected for the specimens with < 10^4 cycles to failure.

The up- and downskin process parameters of the initial six specimens were adjusted to intentionally create a higher surface roughness in the reduced section of the specimens. However, the resulting difference in surface roughness did not result in different fatigue results, as the results of the initial six specimens (see blue markers) are comparable to the HCF results of the validation set. This may be explained by the fact that crack nucleation occurred from defect pores that are much larger than the average surface roughness and likely also larger than the roughness peaks and valleys. Moreover, the defect pores are also larger than the contour region width; hence, spanning into the specimen's core region. The core region was built using the same process parameter set for all specimens. Hence, the same defect size distribution is expected for the initial six specimens as well as for the validation set. For a lognormally distributed defect size it is expected that the average slope of the *S-N* curve goes through the pivot point, which is indeed the case for the HCF specimens of the validation set (see Figure 7).

This paper has demonstrated that for metal LPBF parts the presented fatigue life prediction methodology can be extended to another test specimen geometry, stress ratio and type of material, i.e. from AlSi10Mg to AlSi7Mg. To account for various surface roughness conditions of steel, a fixed stress at 1000 cycles on fully-reversed *S-N* curves, and a change in slope and endurance limit depending on the surface finish have long been used in engineering design guidelines [9-11]. In the current methodology, the pivot point is optimized resulting in a similar number of cycles to failure for the reference point of AlSi7Mg compared to the surface finish methodology for steel; i.e. 1509 cycles and 1000 cycles for AlSi7Mg and steel, respectively. As the presented fatigue life prediction methodology gives similar results using the measured *S-N* data points as well as fractography, it is expected that the applicability of the model can be extended to other alloy systems, fabrication methods and defect types. For Ti-6Al-4V test coupons produced via LPBF and plate-material aluminium 7075-T7351 with corrosion pits, unpublished in-house lab testing results with a stress ratio of $R = 0.1$ has already shown good accordance to the presented methodology. Results shown that indeed a, b and N_{pivot} are constants that only apply for a given material, processing route, specimen geometry, stress ratio, and defect type (e.g. surface finish or LPBF porosity) and its location. Although it is expected that the influence of specimen geometry is limited and the influence of the stress ratio can be incorporated using conventional methodologies for determining the effect of stress ratio on the *S-N* curve.

4. Conclusions

It has been shown that the presented fatigue life prediction methodology for metal LPBF parts can be extended to another material, test specimen geometry and stress ratio. Based on the to-be-applied maximum cyclic stress and the initial defect size within a LPBF part, the fatigue performance can be predicted within statistic confidence bounds.

Experimental results demonstrate that a successful correlation can be achieved between measured and predicted fatigue lives for ‘as built’ AlSi7Mg test specimens under a fully-reversed cyclic loading condition. The model uses the cycles to failure of the pivot point, where the initial defect size has no influence on the fatigue life, as the single fit parameter together with an experimental data set to correlate the assessed fatigue life and associated initial defect size. In this case, the defect pore sizes were much larger than the surface roughness for both the adjusted up- and downskin parameter set and the material-optimized parameter set.

The average *S-N* curve of the 41 fatigue-tested samples of the validation set, for which a similar defect size distribution of the core region is expected based on the usage of similar process parameters, goes through the pivot point that was determined a priori using an initial small set of six specimens.

As the method is capable of predicting fatigue life for various materials, shapes, surface finishes and loading conditions makes this approach a valuable instrument for the industrial application of critically-loaded LPBF components. The use of a priori non-destructive part evaluation techniques and statistically proven allowable defect values result in less scrap and higher productivity. In future work, we believe that by expanding to more materials and further development of empirical data sets, light can be shed on the possibility of ab initio modelling of the two constants a and b of the currently statistically determined slope function.

Acknowledgements

Part of this work was performed when Dr. Wits was still affiliated to Thales Netherlands. His former colleagues of the Thales Group are acknowledged.

References

[1] Thompson MK, et al. Design for Additive Manufacturing: Trends, opportunities, considerations, and constraints. CIRP Annals 2016;65(2):737-760.
[2] Vaneker T, et al. Design for additive manufacturing: Framework and methodology. CIRP Annals 2020;69(2):578-599.
[3] Afroz L, et al. Fatigue behaviour of laser powder bed fusion (L-PBF) Ti–6Al–4V, Al–Si–Mg and stainless steels: a brief overview. International Journal of Fracture 2022; 235(1):3-46.
[4] Jensen SC, et al. Optimization of stochastic feature properties in laser powder bed fusion. Additive Manufacturing 2022;56:102943.
[5] Sanaei N and Fatemi A. Defects in additive manufactured metals and their effect on fatigue performance: A state-of-the-art review. Progress in Materials Science 2021;117:100724.
[6] Zhan Z, et al. Recent developments and future trends in fatigue life assessment of additively manufactured metals with particular emphasis on machine learning modeling. Fatigue and Fracture of Engineering Materials and Structures 2023;46(12):4425-4464.
[7] Wits WW, Scolaro E, Amsterdam E and Clare AT. The role of scan strategies in fatigue performance for laser powder bed fusion. CIRP Annals 2022;71(1):185-188.
[8] Romano S, et al. Fatigue properties of AlSi10Mg obtained by additive manufacturing: Defect-based modelling and prediction of fatigue strength. Engineering Fracture Mechanics 2018;187:165-189.
[9] Wits WW and Amsterdam E. Fatigue prediction and life assessment method for metal laser powder bed fusion parts. CIRP Annals 2023;72(1):129-132.
[10] Bannantine JA, Comer JJ and Handrock JL. Fundamentals of metal fatigue analysis. Englewood Cliffs, NJ, Prentice Hall, 1990.
[11] McKelvey SA and Fatemi A. Surface finish effect on fatigue behavior of forged steel. International Journal of Fatigue 2012;36(1):130-145.
[12] Hwang WJ, Bang GB and Choa S-H. Effect of a stress relief heat treatment of AlSi7Mg and AlSi10Mg alloys on mechanical and electrical properties according to silicon precipitation. Metals and Materials International 2023;29(5):1311-1322.
[13] Li Z, et al. A fatigue life estimation approach considering the effect of geometry and stress sensitivity. Theoretical and Applied Fracture Mechanics 2021;112:102915.
[14] Yadollahi A and Shamsaei N. Additive manufacturing of fatigue resistant materials: Challenges and opportunities. International Journal of Fatigue 2017;98:14-31.
[15] Domfang Ngnekou JN, et al. Fatigue properties of AlSi10Mg produced by additive layer manufacturing. International Journal of Fatigue 2019;119:160-172.
[16] Amsterdam E, et al. The effect of crack length and maximum stress on the fatigue crack growth rates of engineering alloys. International Journal of Fatigue 2022;161:106919.
[17] Kumar MS, et al. Impact of print orientation on morphological and mechanical properties of L-PBF based AlSi7Mg parts for aerospace applications. Silicon 2022;14(12):7083-7097.